Global Change Biology

Global Change Biology (2016) **22**, 3427–3443, doi: 10.1111/gcb.13305

Regional atmospheric CO_2 inversion reveals seasonal and geographic differences in Amazon net biome exchange

CAROLINE B. ALDEN[1,2], JOHN B. MILLER[3,4], LUCIANA V. GATTI[5], MANUEL M. GLOOR[6], KAIYU GUAN[1], ANNA M. MICHALAK[7], INGRID T. VAN DER LAAN-LUIJKX[8], DANIELLE TOUMA[1], ARLYN ANDREWS[3], LUANA S. BASSO[5], CAIO S. C. CORREIA[5], LUCAS G. DOMINGUES[5], JOANNA JOINER[9], MAARTEN C. KROL[8,10,11], ALEXEI I. LYAPUSTIN[9], WOUTER PETERS[8,12], YOICHI P. SHIGA[7,13], KIRK THONING[3], IVAR R. VAN DER VELDE[12], THIJS T. VAN LEEUWEN[10,11], VINEET YADAV[14] and NOAH S. DIFFENBAUGH[1,2]

[1]*Department of Earth System Science, Stanford University, Stanford, CA 94305, USA,* [2]*Woods Institute for the Environment, Stanford University, Stanford, CA 94305, USA,* [3]*Global Monitoring Division, Earth System Research Laboratory, National Oceanic and Atmospheric Administration, 325 Broadway, Boulder, CO 80305, USA,* [4]*Cooperative Institute for Research in Environmental Sciences (CIRES), University of Colorado, Boulder, CO 80309, USA,* [5]*Instituto de Pesquisas Energéticas e Nucleares (IPEN)-Comissao Nacional de Energia Nuclear (CNEN)-Atmospheric Chemistry Laboratory, 2242 Avenida Professor Lineu Prestes, Cidade Universitaria, Sao Paulo CEP 05508-000, Brazil,* [6]*School of Geography, University of Leeds, Woodhouse Lane, Leeds LS9 2JT, UK,* [7]*Department of Global Ecology, Carnegie Institution for Science, Stanford, CA 94305, USA,* [8]*Department of Meteorology and Air Quality, Wageningen University, PO Box 47, 6700AA Wageningen, The Netherlands,* [9]*National Aeronautics and Space Administration, Goddard Space Flight Center, Greenbelt, MD 20771, USA,* [10]*Institute for Marine and Atmospheric Research Utrecht, Utrecht University, Princetonplein 5, 3584 CC Utrecht, The Netherlands,* [11]*SRON Netherlands Institute for Space Research, Sorbonnelaan 2, 3584 CA Utrecht, The Netherlands,* [12]*University of Groningen, Centre for Isotope Research, Nijenborgh 4, 9747AG Groningen, The Netherlands,* [13]*Department of Civil and Environmental Engineering, Stanford University, Stanford, CA 94305, USA,* [14]*Jet Propulsion Laboratory, California Institute of Technology, Pasadena, CA 91109, USA*

Abstract

Understanding tropical rainforest carbon exchange and its response to heat and drought is critical for quantifying the effects of climate change on tropical ecosystems, including global climate–carbon feedbacks. Of particular importance for the global carbon budget is net biome exchange of CO_2 with the atmosphere (NBE), which represents nonfire carbon fluxes into and out of biomass and soils. Subannual and sub-Basin Amazon NBE estimates have relied heavily on process-based biosphere models, despite lack of model agreement with plot-scale observations. We present a new analysis of airborne measurements that reveals monthly, regional-scale (~1–8 $\times$ 10^6 km^2) NBE variations. We develop a regional atmospheric CO_2 inversion that provides the first analysis of geographic and temporal variability in Amazon biosphere–atmosphere carbon exchange and that is minimally influenced by biosphere model-based first guesses of seasonal and annual mean fluxes. We find little evidence for a clear seasonal cycle in Amazon NBE but do find NBE sensitivity to aberrations from long-term mean climate. In particular, we observe increased NBE (more carbon emitted to the atmosphere) associated with heat and drought in 2010, and correlations between wet season NBE and precipitation (negative correlation) and temperature (positive correlation). In the eastern Amazon, pulses of increased NBE persisted through 2011, suggesting legacy effects of 2010 heat and drought. We also identify regional differences in postdrought NBE that appear related to long-term water availability. We examine satellite proxies and find evidence for higher gross primary productivity (GPP) during a pulse of increased carbon uptake in 2011, and lower GPP during a period of increased NBE in the 2010 dry season drought, but links between GPP and NBE changes are not conclusive. These results provide novel evidence of NBE sensitivity to short-term temperature and moisture extremes in the Amazon, where monthly and sub-Basin estimates have not been previously available.

Keywords: Amazon, climate extremes, CO_2, inverse model, terrestrial biosphere, tropical carbon exchange

Received 11 September 2015 and accepted 25 March 2016

Introduction

The Amazon has been identified as a highly climate-sensitive ecosystem, where forest dieback could cause local biodiversity loss and massive release of carbon to

Correspondence: Caroline Alden, tel. +1 719 930 5281, fax +1 303 492 3498, e-mail: aldenc@colorado.edu

the atmosphere, along with changes in regional and global atmospheric conditions (Cox *et al*., 2000; Silva Dias *et al*., 2002; Betts *et al*., 2008; Sitch *et al*., 2008). Understanding Amazon net biome exchange of CO_2 with the atmosphere, and the response of CO_2 fluxes to climate variability and change, is therefore critical for predicting land carbon stability and global climate feedbacks (Cox *et al*., 2000; Sitch *et al*., 2008). Anthropogenic climate change is expected to alter extreme heat (Diffenbaugh & Scherer, 2011) and dry period length and severity (Li *et al*., 2006; Marengo *et al*., 2011; Lintner *et al*., 2012) in the Amazon. Sustained warm events have already been observed, especially in conjunction with severe droughts (Diffenbaugh & Scherer, 2011; Toomey *et al*., 2011; Jiménez-Muñoz *et al*., 2013). However, uncertainty about the effects of increasing climate extremes on the long-term state of forest ecosystems, and on CO_2 sink strength in particular, remains high (Phillips *et al*., 2009; Toomey *et al*., 2011; Frank *et al*., 2015).

Previous efforts to quantify nonfire net biome exchange (NBE) of CO_2 between the atmosphere and tropical rainforests have been limited in several ways. Plot and eddy flux studies are restricted in spatial extent and are therefore insufficient to characterize forest carbon exchange over regional or Basin-wide scales ($\sim 1 \times 10^6$ km^2 to $\sim 8 \times 10^6$ km^2) (Araújo *et al*., 2002). Past atmospheric inversion modeling efforts have made estimating tropical CO_2 exchange at large scales possible, but different inverse models have not agreed on the sign or strength of the tropical South American carbon balance, primarily due to a lack of observations in and sensitive to the Amazon (Gurney *et al*., 2002; Peylin *et al*., 2013). More recent studies, using new atmospheric CO_2 observations in the Amazon, calculated NBE fluxes at the Basin scale (Gatti *et al*., 2014; van der Laan-Luijkx *et al*., 2015) leaving temporal and spatial detail largely unresolved. Finally, past atmospheric transport inversions for net CO_2 fluxes in the Amazon have been dependent on flux estimates from process-based models, despite the failure of those models to properly simulate either the observed seasonality of fluxes (Saleska *et al*., 2003; Baker *et al*., 2009) or the observed impacts of drought (Powell *et al*., 2013; Joetzjer *et al*., 2014). The lack of independent temporally and spatially resolved constraints on Amazon fluxes has meant that little has been known about net carbon exchange with the atmosphere at monthly timescales and regional spatial scales.

The period 2010–2012 spans a particularly interesting suite of years for studying net exchange of carbon between the Amazon biosphere and the atmosphere, because of the unusual climate conditions that occurred during that period. In 2010, a major drought and unusually high temperatures affected much of the Basin (Lewis *et al*., 2011; Jiménez-Muñoz *et al*., 2013), whereas drought indices in 2011 and 2012 were closer to the long-term climatic mean. We calculate NBE in the Amazon for this 3-year period, in a regional Bayesian atmospheric transport inversion, in order to investigate several major questions, including: (1) What is the spatial and temporal variability of Amazon NBE? (2) At regional scales, does Amazon NBE follow a consistent seasonal pattern from year to year, as process-based biosphere models predict? (3) Do drought and heat extremes affect net exchange of CO_2 between the land and atmosphere in the Amazon? (4) If heat and drought impacts on NBE are observable, are these effects consistent across the Amazon Basin, or are there regional differences in response? (5) Can independent satellite proxies for gross primary productivity (GPP) offer evidence that observed changes in the Amazon carbon sink are driven by changes in photosynthesis vs. other terrestrial surface fluxes?

Materials and methods

We present a regional Bayesian inversion that calculates 3-hourly and 1°×1° net fluxes of CO_2, with *a posteriori* covariance, in the Amazon Basin. Based on the inversion results and the degrees of freedom offered by the atmospheric observations, we interpret fluxes at the monthly scale for 5 regions of the Amazon. Our flux calculation method is largely independent of prior 'bottom-up' model estimates of sink strength, spatial pattern of fluxes, and seasonality of fluxes. We quantify nonfire net biome exchange of CO_2 ('NBE') at high temporal and geographic resolution using *in situ* CO_2 vertical profiles collected by aircraft from 2010 to 2012. Fire emission estimates are from an atmospheric CO inversion (van der Laan-Luijkx *et al*., 2015). Unique aspects of this inversion are (1) relative independence from biosphere model NBE estimates and (2) observationally constrained calculation and optimization of the background CO_2 concentration over the tropical Atlantic. To minimize uncertainties arising from atmospheric transport, we focus on relative and month-on-month changes in NBE and use two different transport models (see *Supporting Information*).

Atmospheric observations

Atmospheric carbon dioxide (CO_2) is sampled by aircraft along a vertical profile over four sites in the Amazon Basin at 2-week intervals in 2010–2012. The four sites are as follows: Alta Floresta (ALF), Rio Branco (RBA), Santarém (SAN), and Tabatinga (TAB) (Fig. 1). Most samples are taken between 11:00 and 14:00 local time (Fig. S1), by which time the previous day's nocturnal stable layer has mixed into the daytime planetary boundary layer. Samples are taken by semiautomatic filling of programmable flask packages; 17 0.7-l flasks are filled for each vertical profile at SAN, and 12 0.7-liter flasks are filled

for each vertical profile at ALF, TAB, and RBA. From 1200 m altitude and higher, samples are taken roughly every 300 m, and below 1200 m altitude, samples are taken roughly every 150 m. CO_2 is measured by nondispersive infrared analysis at the Instituto de Pesquisa Energéticas Nucleares (IPEN) Atmospheric Chemistry Laboratory in São Paulo. A full description of sample recovery, analysis, repeatability, and reproducibility can be found in Gatti *et al.* (2014).

Bayesian atmospheric inversion model

Atmospheric CO_2 inversions use spatial and temporal gradients in atmospheric CO_2 concentrations to estimate net surface-to-atmosphere fluxes of CO_2. An atmospheric transport model links atmospheric observations to surface fluxes, and prior knowledge of fluxes and uncertainties constrain the result. Flux estimation is performed by Bayesian inversion, with assumptions of Gaussian error distribution (Tarantola, 1987; Rodgers, 2000). An optimal estimate of fluxes can be found by minimizing the cost function, L_s, which is the sum of modeled and observed CO_2 differences weighted by the model–data mismatch term, **R**, and prior and optimized flux differences weighted by the flux uncertainty term, **Q**:

$$L_s = (\mathbf{z} - \mathbf{Hs})^T \mathbf{R}^{-1} (\mathbf{z} - \mathbf{Hs}) + (\mathbf{s} - \mathbf{s}_p)^T \mathbf{Q}^{-1} (\mathbf{s} - \mathbf{s}_p) \quad (1)$$

z is an $n \times 1$ vector of atmospheric observations, and **R** is an $n \times n$ diagonal matrix (covariance is not considered) representing model–data mismatch, or expected uncertainty in how well modeled CO_2 concentrations match true CO_2 concentrations (Tarantola, 1987; Engelen *et al.*, 2002). **H**, which is derived from transport models, is an $n \times m$ matrix of surface influence functions, or the sensitivity of each measurement to surface fluxes. $\mathbf{s}_p$ is an $m \times 1$ vector of the prior estimate of surface-to-atmosphere fluxes of CO_2, **Q** is an $m \times m$ matrix of prior flux uncertainties, and **s** is an $m \times 1$ vector of true surface-to-atmosphere CO_2 fluxes (Tarantola, 1987).

Dimension n is the total number of observations (n = 976 in 2010, n = 917 in 2011, and n = 926 in 2012), and m is the total number of surface flux values being estimated (spatial resolution of 1487 land grid cells by temporal resolution of 2920 3-hourly time steps in a nonleap year), plus n estimates of background CO_2. One background CO_2 estimate for each observation is appended to the state vector for optimization in the inversion. In this framework, m = 1487 grid cells × 2920 time steps + n background CO_2 values.

Minimizing the objective function in Eqn. 1 results in a solution for $\hat{\mathbf{s}}$, an $m \times 1$ vector of posterior fluxes (Tarantola, 1987):

$$\hat{\mathbf{s}} = \mathbf{s}_p + \mathbf{QH}^T (\mathbf{HQH}^T + \mathbf{R})^{-1} (\mathbf{z} - \mathbf{Hs}_p) \quad (2)$$

We assess the posterior flux uncertainty, $\mathbf{V}_{\hat{\mathbf{s}}}$, which can be calculated as the inverse of the Hessian of L_s. The posterior flux covariance matrix, $\mathbf{V}_{\hat{\mathbf{s}}}$, is a useful metric for assessing uncertainty and covariance of the flux results.

$$\mathbf{V}_{\hat{\mathbf{s}}} = \mathbf{Q} - \mathbf{QH}^T (\mathbf{HQH}^T + \mathbf{R})^{-1} \mathbf{HQ} \quad (3)$$

Inversions and posterior uncertainty calculations are performed using the computational efficiency techniques of Yadav & Michalak (2013). Using these techniques, we calculate $\mathbf{V}_{\hat{\mathbf{s}}}$ analytically, not by approximation, as is typically done for calculations with these dimensions.

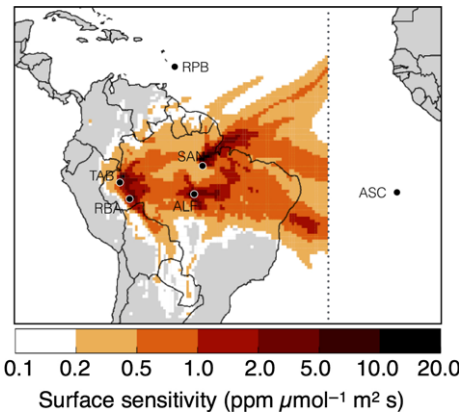

Fig. 1 Measurement sites and surface sensitivity to 2011 observations. Black dots indicate aircraft measurement sites, Rio Branco (RBA), Alta Floresta (ALF), Tabatinga (TAB), and Santarem (SAN), as well as two background sites, Ragged Point, Barbados (RPB) and Ascension Island (ASC), that are part of the NOAA/ESRL network. The dotted line at −30° longitude is the regional inversion boundary domain, where background CO_2 is estimated. Orange shading shows the total surface sensitivity to all measurements made at Amazonian sites in the year 2011, plotted on a log scale.

Model inputs and uncertainties

Transport models. Surface influence functions (**H**) are calculated using two Lagrangian particle dispersion models: Flexpart version 9.0 with 0.5 degree Global Forecast System (GFS) meteorology and 7-day back trajectories (Stohl *et al.*, 2005), and Hysplit with 0.5 degree Global Data Assimilation System (GDAS) meteorology (Draxler & Hess, 1998) and 10-day (the decision of the group who runs this model) back trajectories. We use both models for uncertainty calculations, and Flexpart for the inversions that produced the results that we show here, based on sensitivity tests and model comparisons (see *Supporting Information*).

Model–data mismatch. The model–data mismatch uncertainty term, **R**, represents estimated error in how closely true atmospheric concentrations of CO_2 can be approximated in the inversion. This uncertainty is due only trivially to measurement-related uncertainty, mainly to uncertainty in modeled atmospheric transport, and additionally to background sampling uncertainty, uncertainty of other surface fluxes of CO_2, and representation uncertainty. Measurement uncertainty includes uncertainty in measurements made at IPEN (±0.1 ppm) and uncertainty in scale between IPEN and NOAA (±0.1 ppm) (Gatti *et al.*, 2014). We compare two Lagrangian particle dispersion models (Flexpart and Hysplit) to estimate transport uncertainty, which is typically ~1–7 ppm (details in *Supporting Information*). Background CO_2 sampling

uncertainty is calculated as the square of the standard deviation of differences between background CO_2 values sampled using Flexpart and Hysplit back trajectories (see *Supplemental Information* for details). Other surface flux uncertainties include those from biomass burning, fossil fuel emission, and net surface ocean flux of CO_2. Footprints from Flexpart are used to propagate biomass burning uncertainty, $\mathbf{Q}_{BB}$, into uncertainty in the atmospheric mole fraction of CO_2 by calculating $\mathbf{HQ}_{BB}\mathbf{H}^T$, where $\mathbf{Q}_{BB}$ is a diagonal matrix of variance in biomass burning emissions (see *Supplemental Information* for details on estimation of $\mathbf{Q}_{BB}$). Following the assumptions above, the diagonal elements of the model–data mismatch from biomass burning uncertainty are added to $\mathbf{R}$. Fossil fuel and ocean fluxes and their uncertainties are small in the Amazon, and representation errors (or effects of model resolution) are not well known. To be conservative, however, we increase the combined 1-sigma uncertainty from all of the above sources by an arbitrary value of 5% to allow for possible combined contributions of uncertainty from those sources.

Prior NBE flux estimate. The surface-to-atmosphere flux that is estimated in the inversion ($\hat{\mathbf{s}}$) is nonfire net biome exchange, F_{NBE}, a term that represents net biosphere–atmosphere exchange of CO_2, including gross primary production, plant (autotrophic) respiration, decomposition (heterotrophic respiration), and disturbance and human land use change (except for biomass burning). We subtract the influences of all other major known sources of CO_2 in the Amazon (fossil fuel emission, net ocean exchange, and biomass burning) from atmospheric observations by multiplying estimates of each CO_2 source by $\mathbf{H}$ and subtracting the resulting atmospheric CO_2 change from observations (see *Supporting Information*). The net source/sink strength of prior F_{NBE} ($\mathbf{s}_p$) is zero on timescales longer than 1 day (i.e., sums of daily, weekly, and annual fluxes are zero with respect to net surface-to-atmosphere CO_2 exchange). Prior F_{NBE} has a diurnal cycle of net uptake of CO_2 by the biosphere during the daytime and net release of CO_2 to the atmosphere at night. The diurnal cycle is unique to each grid cell, reflecting spatial heterogeneity in Amazon NBE, and is calculated as the annual mean diurnal cycle from SiBCASA (with the mean subtracted) for the year 2011 (Schaefer *et al.*, 2008; van der Velde *et al.*, 2014). Detailed discussion of the prior flux estimate and a test of posterior flux sensitivity to $\mathbf{s}_p$ can be found in the *Supporting Information*.

NBE flux uncertainty. The diagonal elements of $\mathbf{Q}$ contain prior flux variance (Eqns. 1–3). Inversion flux calculations are sensitive to the choice of prior flux uncertainty (Gerbig *et al.*, 2006; Gourdji *et al.*, 2012). Of particular importance for our experimental design is that prior flux uncertainty is large enough that the posterior flux estimate can diverge from the neutral prior flux estimate. We vary prior F_{NBE} uncertainty with 1° by 1° in space, but not in time, since the seasonality of Amazon flux uncertainty is not known, and because varying F_{NBE} uncertainty in time could affect temporal variability of the posterior flux. The time resolution of the inversion is 3-hourly, which means that the full amplitude of the diurnal cycle of CO_2 is represented in the prior flux uncertainty estimate. The amplitude of the diurnal cycle of NBE in the Amazon is thought to be of a similar order of magnitude as the gross photosynthetic and respiration fluxes (e.g., Powell *et al.*, 2013), and those component fluxes are thought to be of similar magnitudes to one another (Malhi *et al.*, 1999). We therefore estimate prior flux variance as the square of 100% of annual mean monthly heterotrophic respiration, from the CASA-GFED v3.1 output (van der Werf *et al.*, 2010). We account for additional uncertainty arising from possible errors in the estimated diurnal cycle of the prior flux, calculated as the square of the standard deviation of the difference between the SiBCASA and CASA-GFED diurnal cycles for each grid cell (see *Supporting Information*).

The off-diagonal elements of $\mathbf{Q}$ represent temporal and spatial correlations of uncertainty in ecosystem carbon exchange (Baldocchi *et al.*, 2001; Michalak *et al.*, 2004; Gerbig *et al.*, 2006). We assume that flux correlations decay isotropically in space and time, with exponential decorrelation length scale parameters of ι_{time} = 5 days and ι_{space} = 300 km (e.g., Yadav & Michalak, 2013). This choice means we assume that fluxes that are closer in space or time have higher uncertainty correlations than do fluxes that are more geographically or temporally separated. Flux covariance in time is limited to the same time step of the diurnal cycle; for example, fluxes in the first time step of Day 1 are correlated with the first time step in the days preceding and following Day 1 (in the limit of the exponentially decaying time correlation constant), but not with any other time of day (Yadav & Michalak, 2013). ι_{space} of 300 km and ι_{time} of 5 days imply that fluxes remain correlated with roughly 3 times those distances (900 km and 15 days), which is approximately the timescale over which synoptic weather patterns vary in the tropics (Madden & Julian, 1972) and the length scale over which climatic and ecosystem regimes vary in the Amazon (Marengo *et al.*, 2011; Restrepo-coupe *et al.*, 2013). It is possible that our choice of ι_{time} is too short, as correlations between flux uncertainties separated by more than ~1 month are possible. In the limit of the absolute values of GPP and respiration being roughly equal, however, fluxes would be neutral and likely to follow synoptic variability, which suggests that 5 days is a reasonable value.

Posterior F_{NBE} uncertainties are calculated using Eqn. 3 for the time steps and spatial scales of interest (i.e., monthly, seasonally, and annually, and Basin-wide and by region), following Yadav & Michalak (2013).

Background CO_2

The prior 'background CO_2', or boundary condition, is the CO_2 concentration of air flowing into the Amazon Basin (Fig. 1). The background CO_2 concentration is removed from observations of CO_2 to isolate surface-to-atmosphere flux signals that originate in the domain. The background CO_2 concentration is estimated in four steps (described in more detail in the *Supporting Information*): (1) A background CO_2 'prior' is calculated by sampling the 3-dimensional (latitude, altitude, time) CO_2 mole fraction output from CarbonTracker version CT2013_ei (Peters *et al.*, 2007; CarbonTracker CT2013B); (2) the background CO_2 'prior' is bias-corrected using *in situ*

measurements of atmospheric CO_2 from two NOAA/ESRL GMD network sites in the Atlantic Ocean; (3) the bias-corrected background CO_2 'prior' is sampled using Lagrangian transport model back trajectories for each observation; and (4) the background CO_2 prior is appended to the state vector, $\mathbf{s}_p$, and is optimized in the inversion.

Two sources of 'background CO_2 construction' uncertainty are accounted for, and are included in the section of the **Q** matrix related to prior background CO_2 uncertainty (which is fully populated and includes covariance terms). Estimation of this source of uncertainty is described in detail in the *Supporting Information*. Correlations between background CO_2 uncertainties decay exponentially and isotropically in space (l_{space} = 1000 km) and time (l_{time} = 7 days), at scales equivalent to ~1/3 the synoptic-scale variability of domain inflow air (Madden & Julian, 1972). An additional source of uncertainty arising from the background inflow of CO_2 is the 'background CO_2 sampling' uncertainty, which is included in the model–data mismatch term, **R** (described above and in the *Supporting Information)*.

Climate and satellite data

We assess drought conditions in the Amazon using two metrics, monthly cumulative water deficit (CWD) and the supply-demand drought index (SDDI), both standardized to reflect anomalies from the long-term climatological mean. We include CWD given its use in the Amazon literature (Aragão *et al*., 2007; Gatti *et al*., 2014; Doughty *et al*., 2015), and we include SDDI in order to provide a potentially more realistic estimation of moisture deficit.

CWD is calculated according to the methods of Aragão *et al.* (2007) (see *Supporting Information* for details), using precipitation data from the Tropical Rainfall Measuring Mission (TRMM) Merged HQ/Infrared Precipitation dataset (Huffman *et al*., 2007). Calculation of CWD uses time and space invariant evapotranspiration, which provides simplicity, but is an unrealistic assumption. A second simplifying assumption of CWD is that the index resets to zero each year, meaning that it does not capture the cumulative effects of precipitation deficits over multiple years. These simplifying assumptions provide motivation for also analyzing the SDDI.

The SDDI quantifies moisture deficit by accounting for current climate conditions as well as the previous month's drought state, using a temperature-based estimate of atmospheric demand for water vapor (Rind *et al*., 1990). We calculate SDDI following the methods of Touma *et al.* (2015) (see *Supporting Information* for details), using monthly gridded precipitation from Global Precipitation Climatology Project (GPCP) (Adler *et al*., 2003), and potential evapotranspiration calculated using the Thornthwaite method (Touma *et al*., 2015) with gridded monthly temperature from NCEP/NCAR Reanalysis 1 (Kalnay *et al*., 1996). Negative values of CWD and SDDI indicate drought conditions, and positive values indicate wet conditions.

Two satellite proxies – solar-induced fluorescence (SIF) and enhanced vegetation index (MAIAC EVI) – are thought to reveal variations in the relative strength of GPP. Estimates of GPP using eddy covariance techniques show high correlations with SIF (Guanter *et al*., 2014; Joiner *et al*., 2014) and EVI (Rahman *et al*., 2005; Sims *et al*., 2006; Kuhn *et al*., 2007; Huete *et al*., 2008). We use SIF calculated from GOME-2 version 26, level 3, and EVI from MAIAC (details regarding data and processing can be found in *Supporting Information*). Positive values of SIF and EVI are proxy indications of higher rates of GPP (greater biome uptake of CO_2).

We define the dry season in each region as those months when long-term (1981–2010) climatological mean GPCP precipitation (Adler *et al*., 2003) is ≤ the lowest quartile of annual long-term mean GPCP precipitation (1981–2010).

Regional analysis

We analyze NBE for 5 regions of the Amazon (Fig. 3) and at the monthly scale, based on the degrees of freedom offered by the observations and surface influence functions (see *Supporting Information* for details).

Results

Model fit to observations

The posterior fluxes result in a much better match to atmospheric observations than the prior fluxes (i.e., $(\mathbf{H\hat{s}} - \mathbf{z})$ is smaller, on average, than $(\mathbf{Hs}_p - \mathbf{z})$). The mean difference and standard deviation are shown in Table 1 and Fig. 2. Furthermore, the posterior bias $(\mathbf{H\hat{s}} - \mathbf{z})$ is close to zero at all sites and in all seasons (Table 1, Fig. 2), and posterior uncertainties were reduced with respect to prior uncertainties (see *Supporting Information*). These metrics indicate model success in adjusting fluxes to better match observations. We observe no evidence of seasonality or other systematic biases in the difference between posterior modeled CO_2 and observed CO_2 $(\mathbf{H\hat{s}} - \mathbf{z})$ (Fig. 2).

Annual Basin-wide NBE

Total annual F_{NBE} for the Amazon Basin shows important differences between years (Fig. 3a). We confirm that Basin-wide NBE was more positive (more of a source to the atmosphere) in 2010 than in 2011 (bar plot in Fig. 3a) (Gatti *et al*., 2014; Doughty *et al*., 2015; van der Laan-Luijkx *et al*., 2015). The difference of 0.28 ± 0.45 PgC that we observe is statistically consistent with the differences of 0.22 ± 0.26 PgC obtained using a mass balance approach (Gatti *et al*., 2014), 0.08–0.26 PgC yr^{-1} using data assimilation (van der Laan-Luijkx *et al*., 2015), and 0.38 PgC (0.22–0.55 PgC) using extrapolated forest plot data (Doughty *et al*., 2015). We find an even greater difference of 0.68 ± 0.45 PgC between 2010 and 2012, meaning that even more carbon was lost to the atmosphere in 2010 than in 2012.

Table 1 Summary of annual mean difference ± standard deviation between simulated and observed CO_2 mole fractions at each site (modeled – observed), for *a priori* (prior) and *a posteriori* (posterior) fluxes, multiplied by footprints (**H**)

	Alta Floresta (ALF)	Rio Branco (RBA)	Santarém (SAN)	Tabatinga (TAB)
2010				
Prior (CO_2)	−2.17 ± 3.64 ppm	−1.42 ± 5.28 ppm	−0.96 ± 1.90 ppm	−1.53 ± 3.42 ppm
Posterior (CO_2)	−0.19 ± 1.58 ppm	−0.17 ± 1.80 ppm	−0.08 ± 1.00 ppm	−0.21 ± 1.80 ppm
2011				
Prior (CO_2)	−1.48 ± 3.24 ppm	−0.48 ± 4.79 ppm	0.06 ± 3.19 ppm	−0.13 ± 4.33 ppm
Posterior (CO_2)	−0.09 ± 1.26 ppm	−0.08 ± 1.68 ppm	0.06 ± 1.38 ppm	−0.08 ± 1.96 ppm
2012				
Prior (CO_2)	−1.14 ± 4.96 ppm	1.40 ± 6.31 ppm	−0.70 ± 4.29 ppm	−1.64 ± 7.74 ppm
Posterior (CO_2)	−0.26 ± 2.28 ppm	0.12 ± 2.52 ppm	−0.33 ± 2.01 ppm	−0.34 ± 2.54 ppm

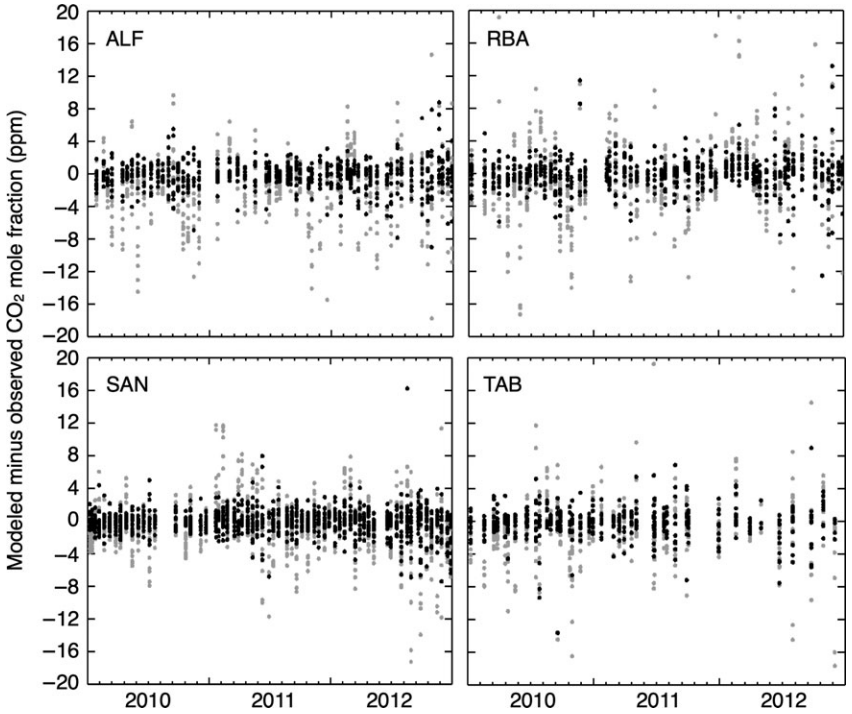

Fig. 2 Differences between prior and posterior simulations of and observed atmospheric CO_2 (simulated–observed). Gray dots are the prior fit to the data ($\mathbf{Hs}_p - \mathbf{z}$). Black dots are the posterior fit to the data ($\mathbf{H\hat{s}} - \mathbf{z}$).

Monthly and seasonal variations in NBE

At the monthly and Basin-wide scale, we observe variations in NBE (±0.04 PgC month^{-1}, 1σ) and differences in seasonal patterns between 2010, 2011, and 2012 (Fig. 3a), suggesting that Amazon NBE shows seasonal variability, but does not exhibit a clearly consistent seasonal cycle during the years studied. Figure 3b shows the definitions of the 5 regions of the Amazon Basin, and Fig. 3c shows NBE for each region. At the scale of wet and dry season variability, consistent patterns of NBE do not emerge in any region (Fig. 4).

The dominant pattern across the basin in 2010 is higher NBE in the wet season (indicating higher carbon losses to the atmosphere), more negative NBE in the dry season, and higher NBE at the end of the year. In 2011 and 2012, however, the seasonal patterns are much different. In general, NBE decreased through 2011 and 2012. One exception is Region 4, where higher carbon uptake in the wet season of 2011 was followed by increased NBE during the rest of the year.

The central Amazon (Region 3) and eastern Amazon (Region 4) show the highest relative CO_2 loss in 2010 (Figs 3c and 4). Sink strength in those two regions also

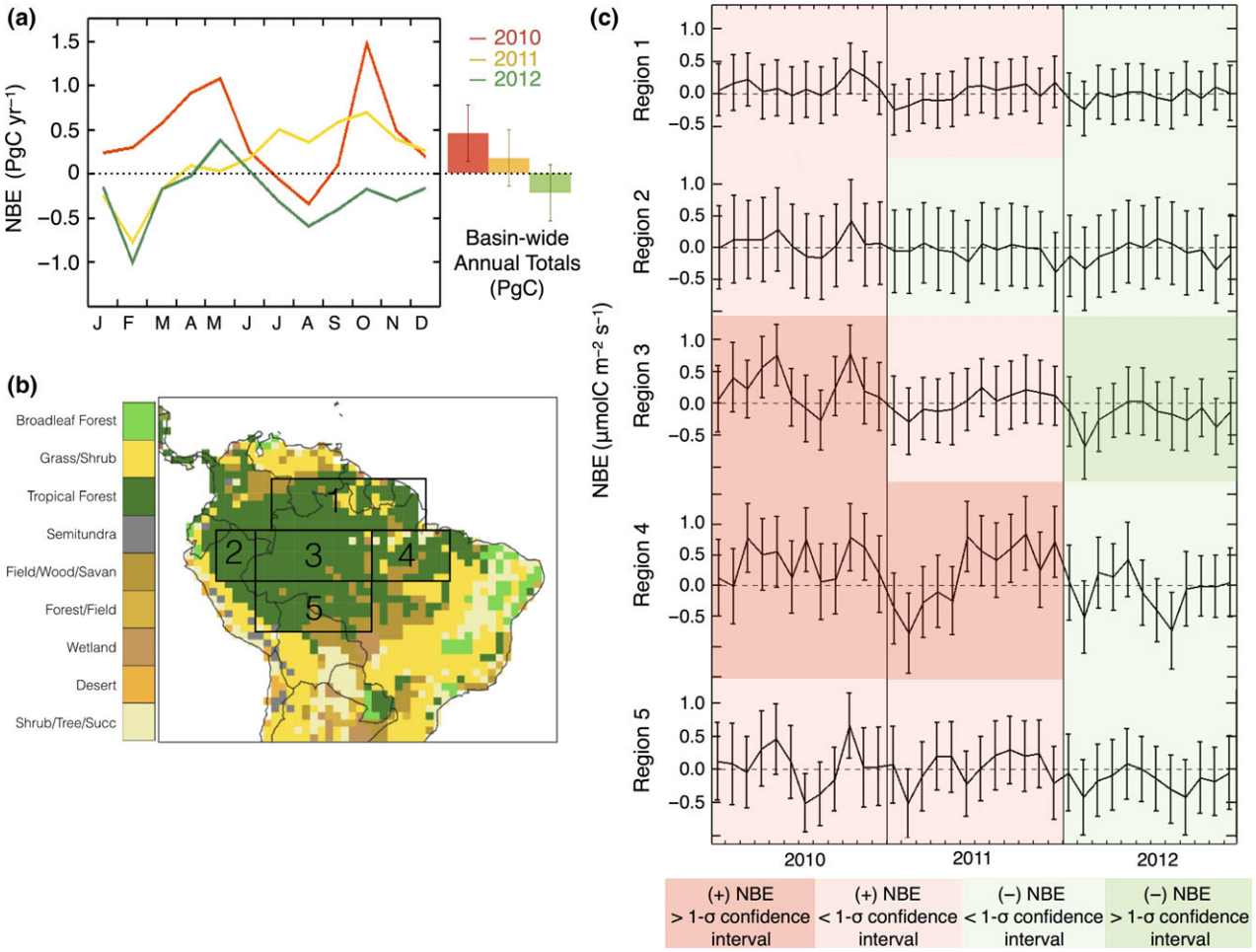

Fig. 3 Basin-wide and regional NBE. (a) Monthly and annual Basin-wide NBE. (b) Region definitions. (c) Regional monthly NBE. (+) NBE indicates source to atmosphere. Uncertainty bars represent 1σ uncertainty in the flux calculation. Shading illustrates sign and confidence of annual mean NBE (see color bar).

exhibits large contrasts between the beginning and end of the record. Furthermore, the meteorological conditions in 2010–2012, combined with the locations and altitudes of the atmospheric CO_2 observations, mean that the observational dataset provides the most information about fluxes in Regions 3 and 4 (Fig. 1, Table S1). This is shown in Fig. 1 as the relative influence of surface fluxes on measured atmospheric mole fractions: Land areas that are close to and upwind of observations provide high influence on those observations. For these reasons, we focus the interpretation of our results on Regions 3 and 4.

Regions 3 and 4 show higher monthly and wet/dry seasonal variability in 2010 and lower variability in 2011–2012, especially in Region 3. Several tests (described in the *Supporting Information*) suggest that this is unlikely to be an artifact of model uncertainty parameterization. Not using a biosphere prior is of primary importance for establishing an independent means of inferring Amazon NBE. It is possible that prior uncertainties are too small, given a neutral prior, to recover seasonality, or that the observations are not dense enough to reliably detect NBE seasonality. We address the first possibility by assigning large prior flux uncertainty and the second possibility by only interpreting fluxes at scales that match the degrees of freedom offered by the observations.

Eastern Amazon wet season

Our record begins during the wet season in 2010, when we find relatively high NBE in the eastern Amazon (indicating higher biosphere-to-atmosphere transfer of carbon) (Fig. 5). Elevated wet season NBE (increased carbon loss) does not appear to be a seasonally recurring pattern in the eastern Amazon (Fig. 5), or anywhere else in the Basin (Figs. 3c and 4). In the eastern Amazon, NBE is much lower in the 2011 wet season

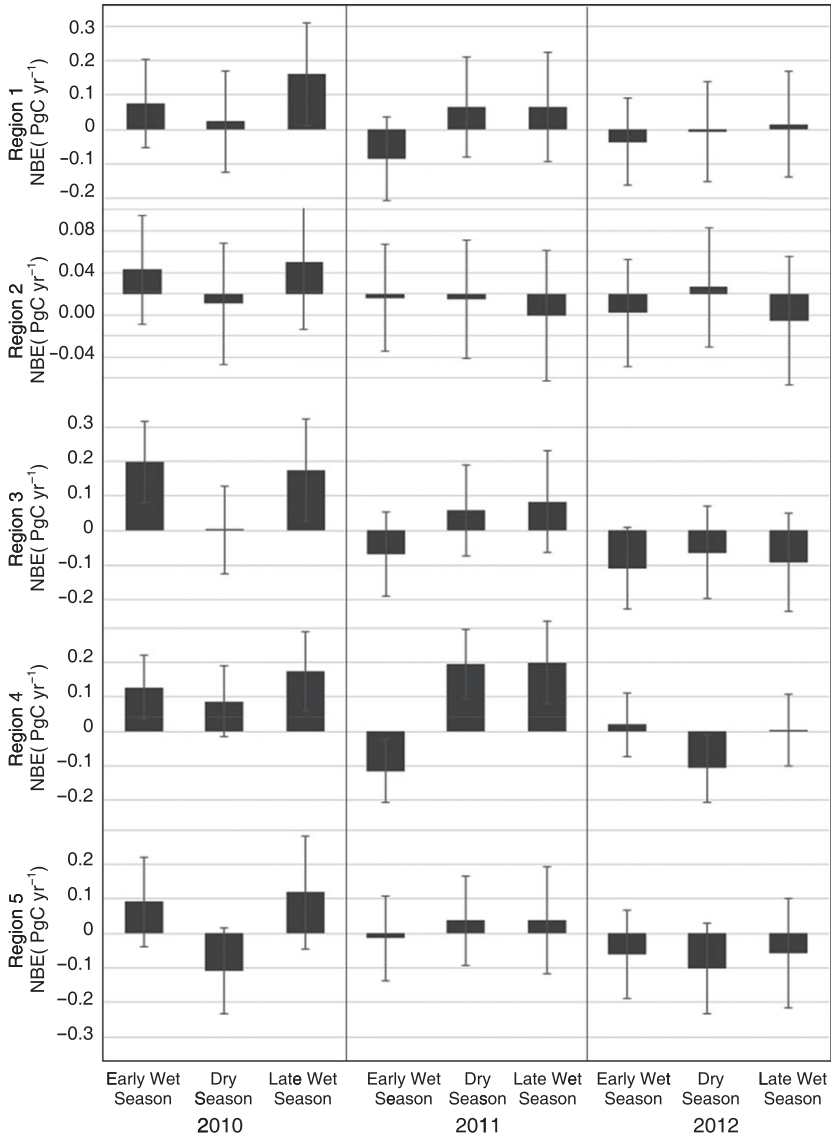

Fig. 4 Wet, dry, and late (October–December) season NBE for each Amazon region.

and closer to neutral in the 2012 wet season. Satellite proxies for GPP in the eastern Amazon do not suggest that lower GPP can explain the wet season NBE increase. SIF and EVI in that year are not consistently higher or lower in the 2010 wet season than in the years following (Fig. 6).

An interesting detail of the 2011 and 2012 wet seasons in the eastern Amazon is a transient shift toward more negative NBE (indicating more carbon uptake by the biosphere) in February. In February 2010, a pause in the multimonth NBE increase is also evident. This pattern suggests a possible recurrence of February uptake, although only a longer record would confirm this pattern. Eastern Amazon EVI and SIF are higher in February 2011 (the month that shows the strongest NBE signal) than in either the 2010 or 2012 wet seasons, suggesting higher GPP in the early 2011 wet season than in the following years.

Precipitation in the eastern Amazon is low during the 2010 wet season compared with the long-term climatological mean. Drought indicators (SDDI and CWD) suggest the onset of eastern Amazon drought conditions in March 2010 (Fig. 5). In that month, precipitation is >2 standard deviations (σ) below the long-term climatological mean (Fig. 5). By contrast, monthly wet season precipitation in 2011 and 2012 is within or marginally above 1 standard deviation of the long-term mean (Fig. 5).

Daily maximum 6-hourly temperature in the eastern Amazon is not remarkably different from the long-term

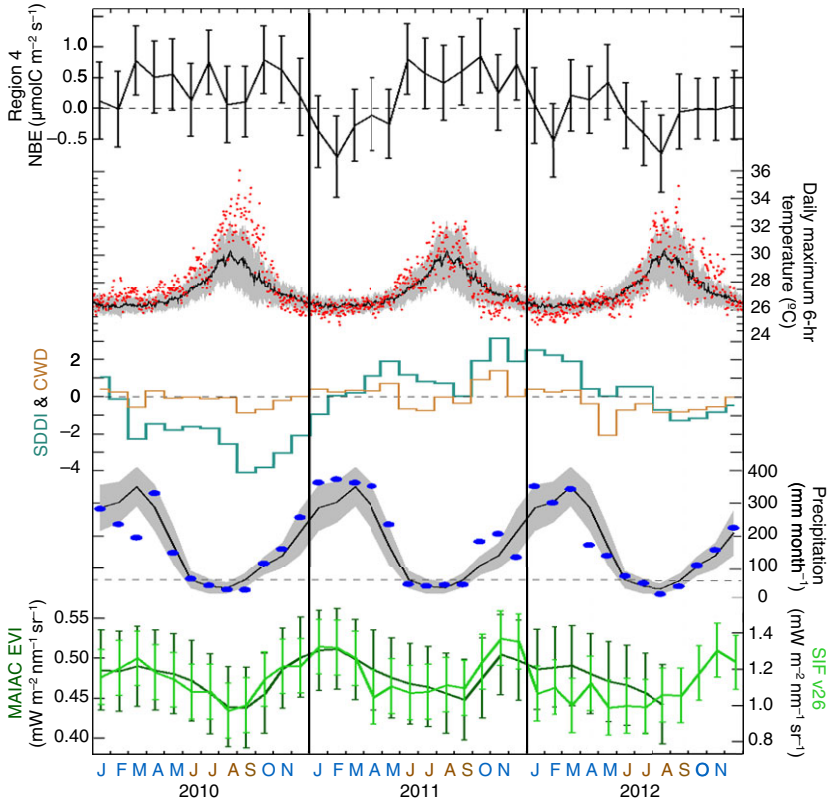

Fig. 5 Eastern Amazon (Region 4) NBE, climate data, and satellite gross primary productivity (GPP) proxies. The top panel shows monthly NBE, with uncertainty bars representing 1σ uncertainty in the flux calculation. The second panel shows daily maximum 6-hourly temperature (red), along with the long-term mean (1981–2010) (black line) and 1σ standard deviation (gray) (Kalnay *et al.*, 1996). The third panel shows the supply-demand drought index (SDDI) (teal) and standardized cumulative water deficit (CWD) (orange), with (−) values indicating drought. The fourth panel shows monthly precipitation (blue), along with the long-term monthly mean (1981–2010) (black) and 1σ standard deviation (gray) (Adler *et al.*, 2003). The bottom panel shows SIF (light-green) and MAIAC EVI (dark-green) with retrieval errors, with higher values of EVI and SIF indicating higher GPP. Names of calendar months are indicated by capital letters across the bottom, with climatological dry season months in brown and other months in blue.

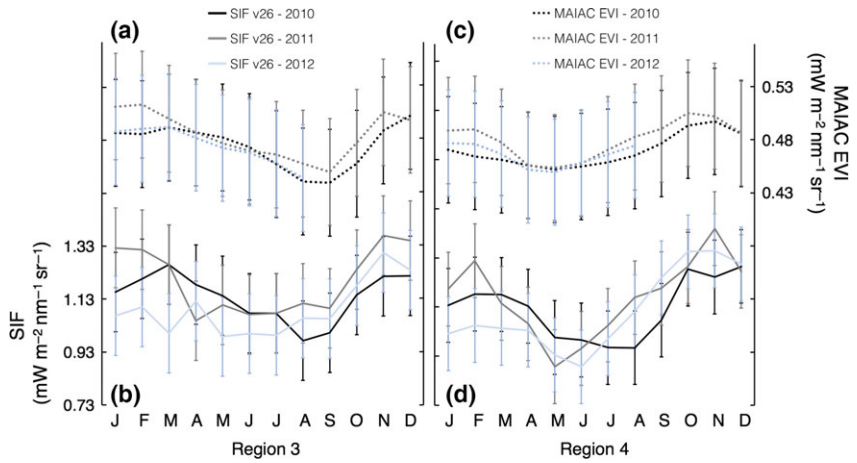

Fig. 6 Monthly MAIAC EVI (top panels) and SIF (bottom panels) overlain for all 3 years of the record, with retrieval uncertainties. (a) Region 3, central Amazon, MAIAC EVI (dotted lines), (b) Region 3, SIF (solid lines), (c) Region 4, eastern Amazon, MAIAC EVI (dotted lines), and (d) Region 4, SIF (solid lines). In all panels, 2010 is black, 2011 is gray, and 2012 is light gray (following legends). Sign conventions: (+) EVI and SIF are proxies for higher photosynthetic uptake (more positive GPP).

mean in the 2010, 2011, or 2012 wet seasons, although conditions may be marginally warmer than the long-term mean in the 2010 wet season and marginally cooler in the 2011 and 2012 wet seasons (Fig. 5).

Eastern Amazon dry season

Eastern Amazon NBE remains relatively high throughout the 2010 dry season (June–September) and is also high in the 2011 dry season (Figs 4 and 5). In 2011, an increase in NBE is evident at the beginning of the dry season, which is notable because it represents an abrupt shift away from more negative values during the wet season. During the 2012 dry season, by contrast, NBE becomes steadily more negative (a shift toward more carbon uptake by the biosphere). In September–November, eastern Amazon NBE is 0.04 ± 0.04 PgC lower in 2012 than in the same months in 2010 (Fig. 5).

Although the 2010 wet season in the eastern Amazon is not particularly hot, the dry season in that region is both very dry and very hot: September precipitation is 54% of normal, and maximum 6-hourly temperature is $>1\sigma$ above the long-term mean in 74% of days in August–September, including $>2\sigma$ above the long-term mean in 23% of days in September. By contrast, in the 2011 dry season, eastern Amazon precipitation is close to 'normal' (107% of the long-term mean). Although some days in the 2011 dry season do exhibit maximum 6-hourly temperature $>1\sigma$ of the long-term mean, hot conditions are far less common and less extreme in 2011, compared with 2010. In 2012, the end of the dry season in the eastern Amazon is again anomalously hot: 39% of days in August–September 2012 exhibit maximum 6-hourly temperature $>1\sigma$ above the long-term mean, and 2% of days are $>2\sigma$ above the long-term mean. SDDI shows the consistently lowest values (indicating dry conditions) of the eastern Amazon record in the 2010 dry season, whereas SDDI is slightly positive in the 2011 dry season and neutral in the 2012 dry season.

Satellite data show higher SIF and EVI in the eastern Amazon in July–December of 2011 than in July–December of 2010 or 2012 (where available), suggesting higher GPP in the latter half of 2011 than in the other years studied (Figs 5 and 6). By contrast, from the end of the dry season to the end of the year in 2010 (August–December), SIF and EVI are much lower than the two following years, indicating lower GPP in the second half of 2010 than in 2011 or 2012 (Figs 5 and 6).

Central Amazon wet season

Central Amazon NBE shows high variability in 2010, but is comparatively stable in 2011 and 2012. It is possible that this result is due to low observational constraint or our use of a neutral prior, although such artifacts would be expected to affect all years equally. Central Amazon NBE shows a steady increase through the 2010 wet season that peaks in May (Fig. 7). In the 2011 wet season, central Amazon NBE is lower than in 2010 (indicating more carbon uptake) (Figs 4 and 7). A negative NBE excursion is observed in February of 2011, although it is not possible to discern the significance of this shift given the statistical uncertainties (Fig. 7). Central Amazon NBE is even lower in the 2012 wet season and shows an abrupt and transient shift toward more negative NBE in February 2012.

Monthly precipitation rates in the 2010 wet season are within 1 standard deviation of the long-term climatological mean. SDDI is high in early 2010 in the central Amazon, likely due in part to normal or wetter than normal precipitation that began in late 2009 (Fig. 7, Fig. S2). Precipitation in 2011 in the central Amazon is also close to the long-term mean, and 2012 is slightly wetter than normal during several months, but the annual mean is 102% of the long-term climatology.

A notable climatic difference between the 2010 wet season and the 2011 and 2012 wet seasons is extreme heat in the central Amazon. In January–May of 2010, 41% of days exhibit maximum 6-hourly temperature $>1\sigma$ above the long-term mean, and 9% of days are $>2\sigma$ above the long-term mean. By contrast, only 4% of days in 2011 and 7% of days in 2012 are $>1\sigma$ above the long-term mean, and less than 1% of days in January–May 2011 or 2012 are greater than 2σ above the long-term climatological mean.

Satellite proxies for GPP in the central Amazon wet season do not show significant differences between years, with the exception of January–February of 2011, when both SIF and EVI are high. This feature is not seen in January–February of 2010 or 2012 (Figs 6 and 7).

Central Amazon dry season

In 2010, the beginning of the central Amazon dry season (June and July) is marked by a shift toward more negative NBE (more carbon uptake by the biosphere) relative to the end of the 2010 wet season. While NBE in the following years does not show a change in sink strength at the end of the wet season, the absolute values of NBE in June–July 2011 and 2012 are similar to the NBE values observed in June–July 2010. In the middle of the 2010 dry season, however, NBE begins to increase again, indicating an increase in net carbon loss to the atmosphere, a feature that is not observed in the dry season in the following years. As a result, September–November NBE is 0.03 ± 0.05 PgC greater in 2010

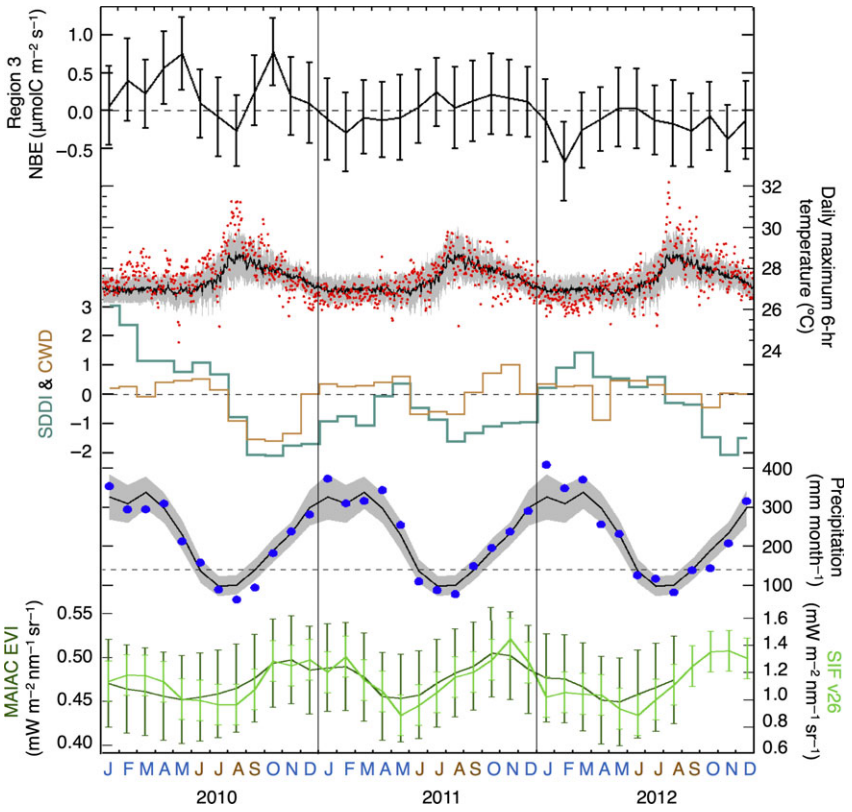

Fig. 7 As in Fig. 5, but for the central Amazon (Region 3).

than in 2011 and 0.08 ± 0.05 PgC greater in 2010 than in 2012 (Fig. 7).

Central Amazon monthly NBE is stable and within 1σ of neutral for all of 2011, suggesting that NBE did not shift more toward a source or a sink during that year (Fig. 7). In 2012, NBE is slightly lower over the length of the dry season, but is not statistically different from 2011 dry season NBE.

In August of the 2010 dry season, NBE shows a sharp increase in the central Amazon at the same time as the onset of drought conditions, according to both the CWD and SDDI (Fig. 7). Central Amazon precipitation is 65% of (and >1σ below) the long-term mean in August–September 2010. In addition, nearly a quarter of days in August show maximum 6-hourly temperature >2σ above the long-term mean, indicating that the central Amazon, like the eastern Amazon, is anomalously hot and dry during the 2010 dry season.

In the 2011 dry season, SDDI is negative, but CWD is not, which suggests that either water deficits from low precipitation in 2010 persisted into 2011 or evapotranspiration is underestimated in CWD for those months. While the 2011 dry season shows mostly 'normal' temperatures, the end of the 2012 dry season is hot: 34% of days show maximum 6-hourly temperature >1σ above the long-term mean in August–September, and 10% of days show temperatures >2σ above the long-term mean. Monthly precipitation in August–September 2012, however, is within 1σ of the long-term climatological mean.

During the first 2 months of the dry season in the central Amazon, SIF and EVI are similar in 2010, 2011, and 2012. In August and September, however, SIF and EVI are substantially lower in 2010 than in August–September of the following 2 years. This suggests lower late dry season GPP in 2010 than in 2011 or 2012. Satellite proxies for GPP do not reveal consistent differences between the 2011 dry season and the 2012 dry season; 2010 is the only clear outlier during this period (Figs 6 and 7).

Discussion

We find month-to-month and year-to-year NBE variability in the Amazon that is small compared with posterior uncertainty. This high uncertainty likely results from conservative choices for uncertainty parameters, as the methods and *Supplemental Information* sections describe. The prior error (and therefore posterior error; $\mathbf{V}_{\hat{\mathbf{s}}}$ depends on $\mathbf{Q}$ (Eqn. 3)) may be overly conservative, and it may therefore be justifiable to interpret the signals in this record more liberally than we do here.

Future investigations of flux uncertainties in the Amazon (e.g., using maximum likelihood techniques (Michalak *et al*., 2005)) or investigation of the 'uncertainty of uncertainties' (e.g., using hierarchical Bayesian methods (Ganesan *et al*., 2014)) could help answer whether our uncertainty limits are overly cautious.

Evidence for seasonality in Amazon NBE

Seasonality in net carbon exchange may be expected in the Amazon, given the strong seasonality in photosynthetically active radiation (PAR) (Restrepo-coupe *et al*., 2013), and the observation, by eddy flux techniques, of seasonal consistency in gross ecosystem productivity that varies according to water limitation across the Basin (Restrepo-coupe *et al*., 2013). Given this consistent wet–dry seasonality (Figs 5 and 7) and seasonality in PAR (Restrepo-coupe *et al*., 2013), one might expect to observe consistent seasonality in NBE from year to year.

A consistent seasonal cycle in NBE is not evident in our 3-year record. A possible exception is wet season (particularly February) increased carbon uptake that occurred in 2011 and 2012 in the eastern and central Amazon, although the signal varies in magnitude and is, at some points, small compared with statistical uncertainty. If February carbon uptake is a seasonally recurring pattern in NBE change, then February 2010 was an anomaly (although the wet season NBE increase paused during that month).

Assuming that the absence of a clear NBE seasonal cycle between years observed in this study does not arise from high uncertainties or low observational constraint, it may indicate higher sensitivity of NBE to short-term climate fluctuations than to seasonal climatology. Because NBE is roughly the difference between GPP and ecosystem respiration, variations in forest carbon balance may be more sensitive to perturbations in GPP and respiration in the tropics (where gross fluxes of carbon into and out of biomass and soil stores remain large year-round (Malhi *et al*., 1999)), compared with the higher latitudes (where seasonal cycles of GPP and respiration dominate the NBE signal (Malhi *et al*., 1999)). It is therefore possible that, in the Amazon, short-term perturbations to GPP and respiration are sufficient to rapidly tip the carbon balance between source and sink. This inference is supported by local-scale eddy covariance studies in the tropics that find large one-way fluxes of CO_2 into and out of the biosphere, but no strong seasonality in net ecosystem exchange of CO_2 (Loescher *et al*., 2003; Goulden *et al*., 2004).

We investigate the possibility that climate anomalies were related to the monthly and interannual variations in NBE in our record. Further, we investigate whether satellite proxies for GPP provide evidence of mechanistic links between observed climate and NBE signals.

NBE and climate anomalies

The large differences in NBE between the years studied (which corroborate other studies of 2010 and 2011) appear to coincide with differences in climate. A major drought affected much of the Amazon Basin in 2010 (Lewis *et al*., 2011; Figs 5 and 7), and NBE was higher in that year than in 2011 or 2012 (Figs 3a and 4): Years that our indices show also had lower drought stress. This apparent relationship between Basin-wide drought and NBE is also evident at regional scales within the Basin. For example, in the eastern Amazon, the increase in NBE (toward a biome carbon source to the atmosphere) in March 2010 coincided with the onset of severe drought conditions (Fig. 5). In July 2010, a period of extreme heat began at the same time as NBE increased again (Fig. 5). Interestingly, in the central Amazon, high wet season NBE observed in 2010 occurred during a period of high temperatures, but not drought stress (Fig. 6). In the late dry season of 2010, however, both drought and high heat accompanied an increase in central Amazon NBE (Fig. 6).

We examine correlations between monthly NBE and anomalies in precipitation and temperature in the wet and dry seasons in both regions. Because relationships between climate and carbon exchange could be subject to lags in response time, we also compare climate data with NBE in the following month.

We found a significant (at the 95% level) negative correlation during the peak wet season (January–April) between NBE and precipitation anomalies (Adler *et al*., 2003) in the eastern Amazon ($R = -0.57$ ($P = 0.05$)) and a less strong correlation in the central Amazon ($R = -0.36$ ($P = 0.25$)) (Fig. 8). We found even stronger correlations between NBE and the previous month's precipitation anomalies in both the eastern and central Amazon ($R = -0.79$ ($P = 0.002$) and $R = -0.52$ ($P = 0.08$), respectively) (Fig. 8). This finding suggests a strong relationship between water inputs and NBE with a possible lag, although temporal correlations between precipitation in consecutive months could explain part of this correlation. Correlations between precipitation and NBE could partly explain why increased February carbon uptake was more strongly pronounced in the nondrought years of our record. It is notable that correlations between precipitation and NBE were strongest in the eastern Amazon, a region that includes savanna, which is highly responsive to rainfall (Santos & Negri, 1997). In the dry season, no clear correlations were found between NBE and

precipitation, except in the central Amazon, when NBE lagged precipitation by 1 month ($R = -0.42$ ($P = 0.18$)).

Correlations between temperature anomalies (Kalnay *et al.*, 1996) and peak wet season NBE were even stronger than correlations with precipitation (central Amazon $R = 0.89$ ($P < 0.001$) and eastern Amazon $R = 0.66$ ($P = 0.02$)). NBE was also correlated with the previous month's temperature anomalies (central Amazon $R = 0.76$ ($P = 0.004$) and eastern Amazon $R = 0.72$ ($P = 0.008$)) (Fig. 9). Again, these correlations could be affected by physical links between climate conditions in consecutive months. No significant correlations were found in the dry season between NBE and temperature (or the previous month's temperature) in either region (Fig. 9).

While our observational dataset does not provide enough information to pursue a rigorous examination of climate impacts and lags greater than weeks to months, it is interesting to speculate whether multiyear impacts of the 2010 drought are evident in our record. For example, if the positive correlation shown in Fig. 8 is not evidence of a direct link between precipitation and NBE, it may instead reveal a multiyear 'recovery' of NBE in the years following drought. More years of data and NBE observations might reveal the cause of these observed correlations, and satellite and plot-scale observations of ecosystem functioning could also provide additional evidence.

Satellite proxies for GPP

We are able examine satellite observations of SIF and EVI concurrent with our record, to look for evidence of changes in GPP that coincide with changes in NBE. During the wet season in the eastern Amazon, NBE was higher in 2010 than in 2011 or 2012. If low GPP had contributed to this increased NBE, then satellite proxies might be expected to show lower SIF and EVI during the 2010 wet season. This signal is not apparent, however, which leaves the possibility that a change in GPP was not the primary contributor to increased NBE during the dry conditions of the 2010 wet season. Similarly, satellite proxies for GPP in the central Amazon do not offer evidence for lower GPP causing high NBE. Instead, it is possible that enhanced respiration was related to high NBE, perhaps related to anomalous heat during that period (Raich & Schlesinger, 1992).

In 2011, January–February NBE indicated higher rates of carbon uptake in the eastern Amazon (and to a lesser extent in the central Amazon). In both the central and eastern Amazon, satellite proxies for GPP were higher in January–February of 2011 than in

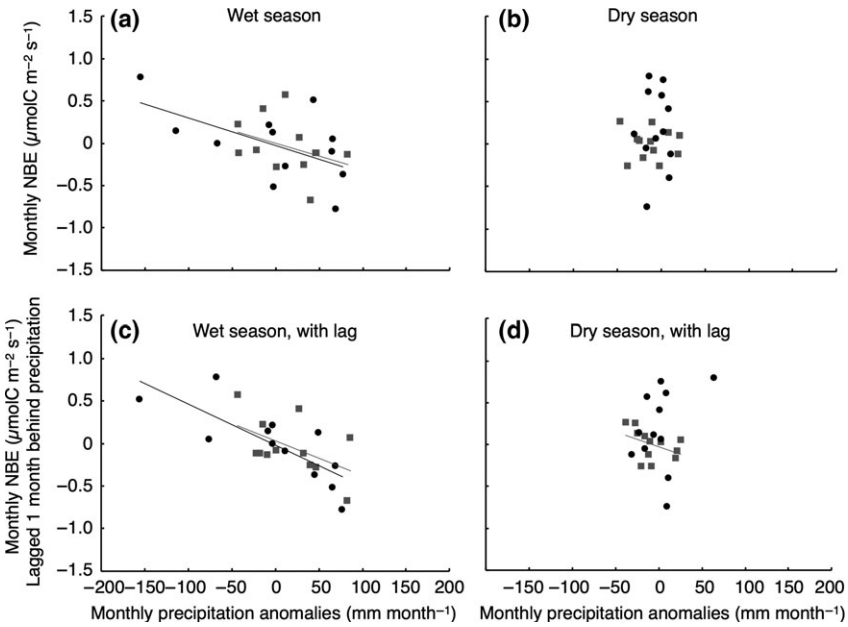

Fig. 8 Correlations between monthly NBE and precipitation anomalies for the central Amazon (gray square) and the eastern Amazon (black dot) in 2010–2012. (a) Wet season (January–April) NBE and precipitation anomalies, central Amazon $R = -0.36$ ($P = 0.25$) and eastern Amazon $R = -0.57$ ($P = 0.05$). (b) Dry season (June–September) NBE and precipitation anomalies, central Amazon $R = -0.06$ ($P = 0.85$) and eastern Amazon $R = 0.03$ ($P = 0.92$). (c) Wet season NBE and previous month's precipitation (December–March precipitation and January–April NBE), central Amazon $R = -0.52$ ($P = 0.08$) and eastern Amazon $R = -0.79$ ($P = 0.002$). (d) Dry season NBE and previous month's precipitation (May–August precipitation and June–September NBE), central Amazon $R = -0.42$ ($P = 0.18$) and eastern Amazon R = 0.32 ($P = 0.32$).

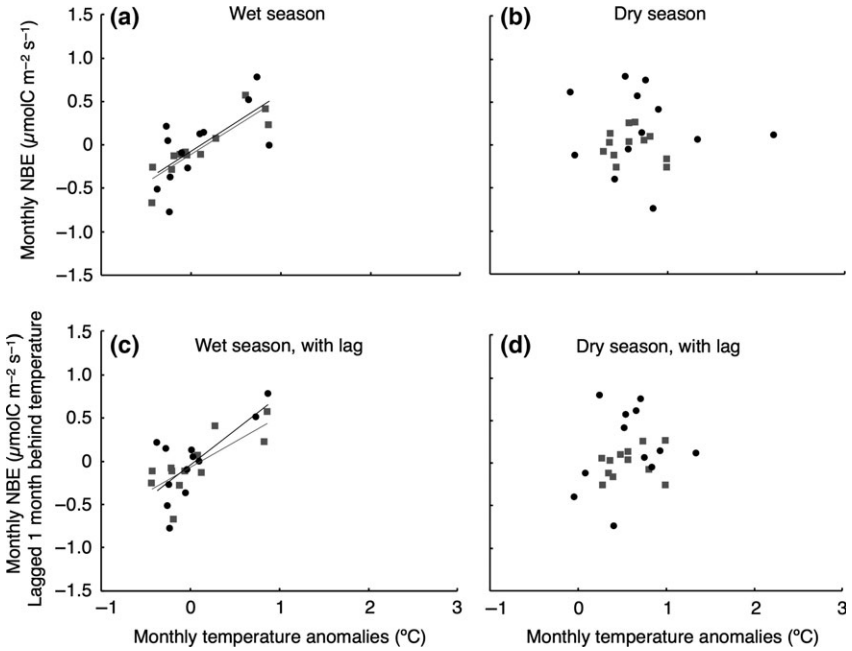

Fig. 9 Correlation between monthly NBE and temperature anomalies for the central Amazon (gray square) and the eastern Amazon (black dot) in 2010–2012. (a) Wet season (January–April) NBE and temperature anomalies, central Amazon $R = 0.89$ ($P < 0.001$) and eastern Amazon $R = 0.66$ ($P = 0.02$). (b) Dry season (June–September) NBE and temperature anomalies, central Amazon $R = -0.17$ ($P = 0.59$) and eastern Amazon $R = 0.02$ ($P = 0.95$). (c) Wet season NBE and previous month's temperature (December–March temperature and January–April NBE), central Amazon $R = 0.76$ ($P = 0.004$) and eastern Amazon $R = 0.72$ ($P = 0.008$). (d) Dry season NBE and previous month's temperature (May–August temperature and June–September NBE), central Amazon $R = 0.25$ ($P = 0.44$) and eastern Amazon $R = 0.20$ ($P = 0.53$).

January–February of 2010 or 2012. NBE and satellite proxies for GPP agree that carbon uptake was high during the 2011 wet season in the eastern Amazon, which suggests that increased GPP may have contributed to decreased NBE. In the central Amazon, however, that relationship is less evident: When central Amazon NBE was at its lowest value of the 3-year record in February of 2012, satellite proxies for GPP were not higher than in the previous years, suggesting that lower NBE is not necessarily related to higher GPP in the central Amazon wet season.

In the beginning of the dry season (June–July), satellite proxies for GPP show no clear difference between years in either the central or eastern Amazon. In the latter half of the dry season, however, August–November SIF and EVI in both regions were lower in 2010 than in 2011 or 2012 (Fig. 6), which suggests that GPP was lower in the late 2010 dry season than in the years following. This period of lower GPP coincided with increased NBE, which indicates that reduced GPP could have contributed to increased carbon losses in the 2010 dry season, a period of extreme heat and drought.

In the 2011 dry season, the observed increase in eastern Amazon NBE did not appear to coincide with decreases in satellite proxies for GPP. If anything, SIF and EVI were higher in the 2011 dry season than in 2010 or 2012. In the 2011 central Amazon dry season, neither NBE nor proxies for GPP showed notable changes. The 2012 dry season was exceptionally hot, but not dry, in the central Amazon, and NBE and GPP were both unremarkable. In the eastern Amazon, a period of decreased eastern Amazon NBE in the 2012 dry season was not accompanied by changes in SIF or EVI.

Neither climatic conditions nor GPP, both of which were 'normal' in the eastern Amazon after February 2011, offers clues to why NBE increased during that period. We posit two possible scenarios for why NBE might have increased in 2011: First, increased biomass mortality during the 2010 drought (Brienen *et al.*, 2015; Doughty *et al.*, 2015), in conjunction with a possible delay in peak mortality following the drought (Doughty *et al.*, 2015), may have provided substrate for decomposition, enabling total respiration to increase as the seasonal cycle warmed in the 2011 dry season (Fig. 5). Second, fire emissions could have been higher than the estimate that we used during the 2011 dry season, which would have resulted in a spurious increase in NBE. However, even the highest biomass burning emission estimates from (van der Laan-Luijkx *et al.*,

2015) cannot explain the NBE increases observed in 2011 (Fig. S3).

If NBE increases in the eastern Amazon in 2011 were related to delayed impacts of the 2010 drought, why did NBE not also increase in the central Amazon in the 2011 dry season? Most regions in the Amazon Basin experienced a progressive decrease in NBE after 2010 (Fig. 3c), but the patterns of NBE change varied: Eastern Amazon NBE decreased more slowly over the 3-year record than Regions 1, 3, and 5, while western Region 2 NBE decreased from higher 2010 values relatively quickly. This spatial pattern generally corresponds with the long-term distribution of soil water availability (Nepstad *et al*., 2004; Fan *et al*., 2013) and seasonally redistributed subsurface water storage (Guan *et al*., 2015), with the fastest recovery occurring where long-term mean soil water availability is greatest (Fig. S4). Both deep plant available water and shallow water table depth are thought to buffer the effects of drought on productivity by allowing forests to maintain soil water availability via redistribution (Nepstad *et al*., 2004; Poulter *et al*., 2009; Fan *et al*., 2013). While other factors such as drought severity, nutrient availability, local climate, impacts of human land use change, and altitude could also explain the gradient in recovery timing, the spatial correspondence suggests the possibility that access to soil water could have at least partially controlled observed changes in the carbon sink over the 3-year period from 2010 to 2012.

Overall, our results reveal possible evidence of sensitivity of the Amazon carbon balance to climate anomalies in 2010–2012, a period of increasingly high temperatures compared with previous decades (Jiménez-Muñoz *et al*., 2013). We suggest that climate variations may have resulted in changes in GPP and respiration that shifted biosphere exchange between sink and source and obscured seasonal patterns in NBE. In particular, it seems possible that a seasonal pattern of early wet season increased carbon uptake (and increased GPP) did not occur in 2010, when heat and drought stress affected much of the Basin.

Whether due to higher drought intensity or higher ecosystem sensitivity, periods of increased NBE lasted through the end of 2011 in the eastern Amazon. The spatial and temporal patterns of recovery across the rest of the Basin may suggest a buffering effect from long-term soil water storage. Water-limited regions in the Amazon are expected to expand in the 21st century (Lintner *et al*., 2012; Pokhrel *et al*., 2014), as is the occurrence of severe heat (Diffenbaugh & Scherer, 2011), which will likely increase the exposure of Amazon forest carbon to hot and dry conditions. Furthermore, negative correlations between wet season NBE and precipitation, and positive correlations between wet season NBE and temperature, suggest increasing risk of ecosystem carbon losses under future climate change scenarios, with potential for lasting carbon climate impacts.

Future analysis and observation of Amazon carbon exchange will help to elucidate the relationships between climate and carbon cycling. A complementary investigation using the geostatistical methods of (Michalak *et al*., 2004) would allow for investigation of correlations between flux intensities and climate parameters (and in comparison with our approach to limiting dependence upon $\mathbf{s}_p$, as geostatistical models do not use a standard prior). Additional trace gas observations, such as $\Delta^{17}O$, carbonyl sulfide (COS) or $\delta^{13}C$ of CO_2, could reveal which component fluxes drive NBE variability, and provide more conclusive links to ecosystem functioning. Finally, there is a need to connect observations collected at different spatial scales in the Amazon – plot, flux tower, tall tower, and our aircraft data – to determine the homogeneity of forest response to climate and the representativeness of observations at different scales.

Acknowledgements

This research was funded by grants from NASA (NNX12AM90G to JBM) and NSF (AGS CAREER 0955283 to NSD). We thank the pilots who collected the air samples, and the measurement analysts and scientists at NOAA for providing data from ASC and RPB. We also thank Sourish Basu and Tyler Jones for helpful discussions and two anonymous reviewers for thoughtful comments and suggestions.

References

Adler RF, Huffman GJ, Chang A *et al*. (2003) The version-2 global precipitation climatology project (GPCP) monthly precipitation analysis (1979–present). *Journal of Hydrometeorology*, **4**, 1147–1167.

Aragão LEOC, Malhi Y, Roman-Cuesta RM, Saatchi S, Anderson LO, Shimabukuro YE (2007) Spatial patterns and fire response of recent Amazonian droughts. *Geophysical Research Letters*, **34**, 1–5.

Araújo A, Nobre AD, Kruijt B *et al*. (2002) Comparative measurements of carbon dioxide fluxes from two nearby towers in a central Amazonian rainforest: the Manaus LBA site. *Journal of Geophysical Research*, **107**, 1–20.

Baker IT, Prihodko L, Denning AS, Goulden M, Miller S, Da Rocha HR (2009) Seasonal drought stress in the Amazon: reconciling models and observations. *Journal of Geophysical Research: Biogeosciences*, **114**, 1–10.

Baldocchi D, Falge E, Gu LH *et al*. (2001) Fluxnet: a new tool to study the temporal and spatial variability of ecosystem-scale carbon dioxide, water vapor, and energy flux densities. *Bulletin of the American Meteorological Society*, **82**, 2415–2434.

Betts R, Sanderson M, Woodward S (2008) Effects of large-scale Amazon forest degradation on climate and air quality through fluxes of carbon dioxide, water, energy, mineral dust and isoprene. *Philosophical Transactions of the Royal Society of London, Series B, Biological Sciences*, **363**, 1873–1880.

Brienen RJW, Phillips OL, Feldpausch TR *et al*. (2015) Long-term decline of the Amazon carbon sink. *Nature*, **519**, 344–348.

CarbonTracker CT2013B. Available at: http://carbontracker.noaa.gov.

Cox PM, Betts RA, Jones CD, Spall SA, Totterdell IJ (2000) Acceleration of global warming due to carbon-cycle feedbacks in a coupled climate model. *Nature*, **408**, 184–187.

Diffenbaugh NS, Scherer M (2011) Observational and model evidence of global emergence of permanent, unprecedented heat in the 20th and 21st centuries. *Climatic Change*, **107**, 615–624.

Doughty CE, Metcalfe DB, Girardin CAJ *et al*. (2015) Drought impact on forest carbon dynamics and fluxes in Amazonia. *Nature*, **519**, 78–82.

Draxler RR, Hess GD (1998) An overview of the HYSPLIT_4 modelling system for trajectories, dispersion, and deposition. *Australian Meteorological Magazine*, **47**, 295–308.

Engelen RJ, Scott DA, Gurney KR *et al*. (2002) On error estimation in atmospheric CO_2 inversions. *Journal of Geophysical Research: Atmospheres*, **107**, 1–13.

Fan Y, Li H, Miguez-Macho G (2013) Global patterns of groundwater table depth. *Science*, **339**, 940–943.

Frank D, Reichstein M, Bahn M *et al*. (2015) Effects of climate extremes on the terrestrial carbon cycle: concepts, processes and potential future impacts. *Global Change Biology*, **21**, 2861–2880.

Ganesan AL, Rigby M, Zammit-Mangion A *et al*. (2014) Characterization of uncertainties in atmospheric trace gas inversions using hierarchical Bayesian methods. *Atmospheric Chemistry and Physics*, **14**, 3855–3864.

Gatti L, Gloor M, Miller JB *et al*. (2014) Drought sensitivity of Amazonian carbon balance revealed by atmospheric measurements. *Nature*, **506**, 76–80.

Gerbig C, Lin JC, Munger JW, Wofsy SC (2006) What can tracer observations in the continental boundary layer tell us about surface-atmosphere fluxes? *Atmospheric Chemistry and Physics*, **6**, 539–554.

Goulden ML, Miller SD, da Rocha HR, Menton MC, de Freitas HC, e Silva Figueira AM, Dias de Sousa CA (2004) Diel and seasonal patterns of tropical forest CO2 exchange. *America*, **14**, 42–54.

Gourdji SM, Mueller KL, Yadav V, Huntzinger DN, Andrews AE, Trudeau M, Petron G (2012) North American CO2 exchange: inter-comparison of modeled estimates with results from a fine-scale atmospheric inversion. *Biogeosciences*, **9**, 457–475.

Guan K, Pan M, Li H *et al*. (2015) Photosynthetic seasonality of global tropical forests constrained by hydroclimate. *Nature Geoscience*, **8**, 284–289.

Guanter L, Zhang Y, Jung M *et al*. (2014) Global and time-resolved monitoring of crop photosynthesis with chlorophyll fluorescence. *Proceedings of the National Academy of Sciences of the United States of America*, **111**, E1327–E1333.

Gurney KR, Law RM, Denning AS *et al*. (2002) Towards robust regional estimates of CO2 sources and sinks using atmospheric transport models. *Nature*, **415**, 626–630.

Huete AR, Restrepo-coupe N, Ratana P, Didan K, Saleska SR (2008) Multiple site tower flux and remote sensing comparisons of tropical forest dynamics in Monsoon Asia. *Agricultural and Forest Meteorology*, **148**, 748–760.

Huffman GJ, Adler RF, Bolvin DT *et al*. (2007) The TRMM Multisatellite Precipitation Analysis (TMPA): quasi-global, multiyear, combined-sensor precipitation estimates at fine scales. *Journal of Hydrometeorology*, **8**, 38–55.

Jiménez-Muñoz JC, Sobrino JA, Mattar C, Malhi Y (2013) Spatial and temporal patterns of the recent warming of the Amazon forest. *Journal of Geophysical Research: Atmospheres*, **118**, 5204–5215.

Joetzjer E, Delire C, Douville H *et al*. (2014) Predicting the response of the Amazon rainforest to persistent drought conditions under current and future climates: a major challenge for global land surface models. *Geoscientific Model Development Discussions*, **7**, 5295–5340.

Joiner J, Yoshida Y, Vasilkov AP *et al*. (2014) The seasonal cycle of satellite chlorophyll fluorescence observations and its relationship to vegetation phenology and ecosystem atmosphere carbon exchange. *Remote Sensing of Environment*, **152**, 375–391.

Kalnay E, Kanamitsu M, Kistler R *et al*. (1996) The NCEP/NCAR 40-year reanalysis project. *Bulletin of the American Meteorological Society*, **77**, 437–471.

Kuhn U, Andreae MO, Ammann C *et al*. (2007) Isoprene and monoterpene fluxes from Central Amazonian rainforest inferred from tower-based and airborne measurements, and implications on the atmospheric chemistry and the local carbon budget. *Atmospheric Chemistry and Physics*, **7**, 2855–2879.

van der Laan-Luijkx IT, van der Velde IR, Krol MC *et al*. (2015) Response of the Amazon carbon balance to the 2010 drought derived with CarbonTracker South America. *Global Biogeochemical Cycles*, **29**, 1092–1108.

Lewis SL, Brando PM, Phillips OL, van der Heijden GMF, Nepstad D (2011) The 2010 Amazon drought. *Science*, **331**, 554.

Li W, Fu R, Dickinson RE (2006) Rainfall and its seasonality over the Amazon in the 21st century as assessed by the coupled models for the IPCC AR4. *Journal of Geophysical Research: Atmospheres*, **111**, 1–14. D02111.

Lintner BR, Biasutti M, Diffenbaugh NS, Lee J-E, Niznik MJ, Findell KL (2012) Amplification of wet and dry month occurrence over tropical land regions in response to global warming. *Journal of Geophysical Research*, **117**, D11106.

Loescher HW, Oberbauer SF, Gholz HL, Clark DB (2003) Environmental controls on net ecosystem-level carbon exchange and productivity in a Central American tropical wet forest. *Global Change Biology*, **9**, 396–412.

Madden R, Julian P (1972) Description of global-scale circulation cells in the tropics with a 40-50 day period. *Journal of the Atmospheric Sciences*, **29**, 1109–1123.

Malhi Y, Baldocchi DD, Jarvis PG (1999) The carbon balance of tropical, temperate and boreal forests. *Plant, Cell and Environment*, **22**, 715–740.

Marengo JA, Tomasella J, Alves LM, Soares WR, Rodriguez DA (2011) The drought of 2010 in the context of historical droughts in the Amazon region. *Geophysical Research Letters*, **38**, 1–5.

Michalak AM, Bruhwiler L, Tans PP (2004) A geostatistical approach to surface flux estimation of atmospheric trace gases. *Journal of Geophysical Research*, **109**, 1–19.

Michalak AM, Hirsch A, Bruhwiler L, Gurney KR, Peters W, Tans PP (2005) Maximum likelihood estimation of covariance parameters for Bayesian atmospheric trace gas surface flux inversions. *Journal of Geophysical Research*, **110**, 1–16.

Nepstad D, Lefebvre P, Da Silva UL *et al*. (2004) Amazon drought and its implications for forest flammability and tree growth: a basin-wide analysis. *Global Change Biology*, **10**, 704–717.

Peters W, Jacobson AR, Sweeney C *et al*. (2007) An atmospheric perspective on North American carbon dioxide exchange: CarbonTracker. *Proceedings of the National Academy of Sciences of the United States of America*, **104**, 18925–18930.

Peylin P, Law RM, Gurney KR *et al*. (2013) Global atmospheric carbon budget: results from an ensemble of atmospheric CO2 inversions. *Biogeosciences*, **10**, 6699–6720.

Phillips OL, Aragão LEOC, Lewis SL *et al*. (2009) Drought sensitivity of the Amazon rainforest. *Science*, **323**, 1344–1347.

Pokhrel YN, Fan Y, Miguez-Macho G (2014) Potential hydrologic changes in the Amazon by the end of the 21st century and the groundwater buffer. *Environmental Research Letters*, **9**, 084004.

Poulter B, Heyder U, Cramer W (2009) Modeling the sensitivity of the seasonal cycle of GPP to dynamic LAI and soil depths in tropical rainforests. *Ecosystems*, **12**, 517–533.

Powell TL, Galbraith DR, Christoffersen BO *et al*. (2013) Confronting model predictions of carbon fluxes with measurements of Amazon forests subjected to experimental drought. *New Phytologist*, **200**, 350–365.

Rahman AF, Sims DA, Cordova VD, El-Masri BZ (2005) Potential of MODIS EVI and surface temperature for directly estimating per-pixel ecosystem C fluxes. *Geophysical Research Letters*, **32**, L19404.

Raich JW, Schlesinger WH (1992) The global carbon dioxide flux in soil respiration and its relationship to vegetation and climate. *Tellus Series B*, **44**, 81–99.

Restrepo-coupe N, Humberto R, Hutyra LR *et al*. (2013) What drives the seasonality of photosynthesis across the Amazon basin? A cross-site analysis of eddy flux tower measurements from the Brasil flux network. *Agricultural and Forest Meteorology*, **182–183**, 128–144.

Rind D, Hansen J, Goldberg R, Rosenzweig C, Ruedy R (1990) Potential evapotranspiration and the likelihood of future drought. *Journal of Geophysical Research*, **95**, 9983–10004.

Rodgers CD (2000) Error analysis and characterisation. *Inverse Methods for Atmospheric Sounding Theory and Practice*, pp. 43–63. World Scientific, Singapore.

Saleska SR, Miller SD, Matross DM *et al*. (2003) Carbon in Amazon forests: unexpected seasonal fluxes and disturbance-induced losses. *Science (New York, N.Y.)*, **302**, 1554–1557.

Santos P, Negri AJ (1997) A Comparison of the normalized difference vegetation Index and rainfall for the Amazon and Northeastern Brazil. *Journal of Applied Meteorology*, **36**, 958–965.

Schaefer K, Collatz GJ, Tans P *et al*. (2008) Combined Simple Biosphere/Carnegie-Ames-Stanford Approach terrestrial carbon cycle model. *Journal of Geophysical Research*, **113**, 1–13.

Silva Dias MAF, Rutledge S, Kabat P *et al*. (2002) Cloud and rain processes in a biosphere-atmosphere interaction context in the Amazon Region. *Journal of Geophysical Research D: Atmospheres*, **107**, 1–18.

Sims DA, Rahman AF, Cordova VD *et al*. (2006) On the use of MODIS EVI to assess gross primary productivity of North American ecosystems. *Journal of Geophysical Research*, **111**, 1–16.

Sitch S, Huntingford C, Gedney N *et al*. (2008) Evaluation of the terrestrial carbon cycle, future plant geography and climate-carbon cycle feedbacks using five Dynamic Global Vegetation Models (DGVMs). *Global Change Biology*, **14**, 2015–2039.

Stohl A, Forster C, Frank A, Seibert P, Wotawa G (2005) Technical note: the Lagrangian particle dispersion model FLEXPART version 6.2. *Atmospheric Chemistry and Physics*, **5**, 2461–2474.

Tarantola A (1987) *Inverse Problem Theory Methods for Data Fitting and Model Parameter Estimation*. Elsevier Sci, New York.

Toomey M, Roberts DA, Still C, Goulden ML, McFadden JP (2011) Remotely sensed heat anomalies linked with Amazonian forest biomass declines. *Geophysical Research Letters*, **38**, 1–5.

Touma D, Ashfaq M, Nayak MA, Kao S-C, Diffenbaugh NS (2015) A multi-model and multi-index evaluation of drought characteristics in the 21st century. *Journal of Hydrology*, **526**, 196–207.

van der Velde IR, Miller JB, Schaefer K, Werf GR, Van Der Krol MC, Peters W (2014) Terrestrial cycling of 13CO2 by photosynthesis, respiration, and biomass burning in SiBCASA. *Biogeosciences*, **11**, 6553–6571.

van der Werf GR, Randerson JT, Giglio L, Collatz GJ, Mu M, Kasibhatla PS, Morton DC (2010) Global fire emissions and the contribution of deforestation, savanna, forest, agricultural, and peat fires (1997–2009). *Atmospheric Chemistry and Physics*, **10**, 11707–11735.

Yadav V, Michalak AM (2013) Improving computational efficiency in large linear inverse problems: an example from carbon dioxide flux estimation. *Geoscientific Model Development*, **6**, 583–590.

Supporting Information

Additional Supporting Information may be found in the online version of this article:

Figure S1. Frequency histograms of the local time of day (in hours since 00:00) for each sample from all sites (ALF, RBA, SAN, and TAB) in 2010, 2011, and 2012.
Figure S2. Central Amazon (Region 3) climate and NBE.
Figure S3. NBE solved in an inversion with influences from fire emissions estimates of (Wiedinmyer *et al*., 2011; Kaiser *et al*., 2012; van der Laan-Luijkx *et al*., 2015) subtracted from the atmospheric observations in Regions 3 (top panel) and 4 (bottom panel).
Figure S4. Panel (a) is reproduced with permission from Figure 4 (their panel c) of (Nepstad *et al*., 2004), showing maximum plant available water at 10 m rooting depth across the Amazon Basin, estimated using soil texture profiles and soil water parameters.
Figure S5. (a) Solid line with circles marking 3-hourly values: the average diurnal cycle for the year 2011, as calculated with the SiB-CASA model, averaged over Region 3 (the central Amazon).
Figure S6. Prior flux (NBE) uncertainty for the year 2010, which equals the sum in quadrature of annual maximum monthly heterotrophic respiration and the standard deviation of differences in the annual mean diurnal cycle calculated with SiBCASA and CASA-GFED.
Figure S7. Monthly NBE for each region (as in Fig. 3); results as for the main results of this work (black lines and posterior uncertainty) and for an inversion run with prior flux uncertainty, σ, doubled (red lines and posterior uncertainty).
Figure S8. Model Data Mismatch (**R**) in units of ppm^2 for each year (all sites).
Figure S9. Monthly mean correlation between Region 3 and Regions 1, 2, 4, and 5 (Fig. 3).
Figure S10. (a) Net ecosystem exchange and biomass burning are shown for each year of the inversion, 2010-2012, as well as for each year of the studies of (Gatti *et al*., 2014) and (van der Laan-Luijkx *et al*., 2015), 2010-2011.
Figure S11. Spearman correlations of the mean seasonal cycles between SIF and MAIAC EVI with BRDF correction (MAIAC EVIn).
Table S1. Table shows, on the diagonal, percent annual mean error reduction by the inversion (from **Q** to $\mathbf{V}_{\hat{\mathbf{s}}}$) in each Region as defined in Fig. 2.
Table S2. Summary of comparisons between transport model ability to simulate vertical concentrations of CO given estimates of biomass burning and background CO.